

# Determination of residual stresses by neutron diffraction in materials and technological components

Franco Rustichelli

Istituto di Scienze Fisiche - Università a degli Studi di Ancona, Via Ranieri 65 - 60131 Ancona

## Abstract

*A review is presented of the non destructive determination of residual stresses by Neutron Diffraction in materials and components of industrial interest. The essential theoretical bases of the techniques are reported. Then a brief description of the experimental facilities is given. Finally several applications of the technique are reported. In particular residual stresses determinations will be presented in welds, thick walled tubes submitted to mechanical pretreatment in order to increase their fatigue life, materials for aerospace technology (gas turbine components and cold expanded holes), metal matrix composites, components for thermonuclear fusion reactor technology submitted to thermomechanical treatments simulating the working conditions of the first wall of the reactor, railway rails after manufacturing process and after service, brazed ceramic-steel components, coatings and fatigue cracked samples. Some comparison between the experimental data and calculations based on finite element technique are presented too.*

## Riassunto

Viene presentata una rivista della determinazione in modo non distruttivo degli sforzi residui mediante Diffrazione Neutronica in materiali e componenti di interesse industriale. Sono riportate le basi teoriche essenziali della tecnica. Quindi viene data una breve descrizione dei dispositivi sperimentali. Infine si riportano diverse applicazioni della tecnica. In particolare si presentano delle determinazioni di sforzi residui in saldature, tubi di grande spessore sottoposti ad un pretrattamento meccanico al fine di aumentare la loro resistenza alla fatica, materiali per la tecnologia aerospaziale (componenti per delle turbine a gas e buchi espansi a freddo), compositi a matrice metallica, componenti per la tecnologia della fusione termonucleare sottoposti a dei trattamenti termomeccanici simulanti le condizioni di lavoro della prima parete del reattore, rotaie dopo il processo di manifattura e dopo esercizio, componenti brasati ceramico-acciaio, ricoprimenti e campioni fratturati da fatica meccanica. Sono altresì presentati dei confronti tra dati sperimentali e calcoli basati sulla tecnica degli elementi finiti.

## INTRODUCTION

Several thermal or mechanical treatments applied to materials and components of technological interest during the manufacturing process can leave residual stresses within the components itself. The residual stresses are defined as the ones which remains in a component when any external force is zero. In particular they arise during the welding or forging processes or in presence of plastic deformation and thermal gradients. Residual stresses can be beneficial or detrimental, depending if they will counteract or not the external loads. When they add to the external loads they can enhance the fatigue process and induce an earlier failure of the component. Anyhow it is very important to know the spatial and directional distribution of residual stresses. Several methods exist so far, some of which are destructive and some other non destructive. Usually mechanical techniques based on strain gauge are destructive as they need that the component be drilled or cut. Some non-destructive techniques are based on acoustic or magnetic effects whereas a peculiar one is based on X-ray diffraction and is very similar to the one based on neutron diffraction. The main difference between these

last two techniques, is that X-ray can be used only in the surface region (depth of few hundreds Ångstroms), due to the strong absorption of this radiation, whereas neutrons can penetrate for several millimeters or centimeters and constitute the most direct technique to measure strains inside a material. On the other hand X-ray can be available in any laboratory, whereas neutrons, at present, are localized in restricted areas where intense and costly neutron sources are available. In any case the stress-induced strains are measured and then the stresses are calculated by knowing the elastic constants of the given material. However the neutron diffraction technique can be used to validate other less accurate but more simple portable methods and finite element calculations. A review will be presented here concerning the **non destructive determination of residual stresses by neutron diffraction** in materials and components of industrial interest. This review is following a very recent one presenting the applications of Small Angle Neutron Scattering in material science and technology [1].

## THEORETICAL BASES

The principle of the strain measurement by neutron diffraction is shown in fig. 1. A monochromatic and collimated neutron beam is diffracted by the polycrystalline sample and pass through a second collimator, which together with the first one define the "gauge" volume, the cross section of which can be so small as  $1 \times 1 \text{ mm}^2$  and in special cases also smaller. By knowing the neutron wavelength  $\lambda$ , and by measuring the  $2\theta$  take-off angle at which the maximum of the Bragg peak occurs, one can evaluate the interplanar distance  $d_{hkl}$  associated to the diffracting crystallographic planes of Miller indices  $hkl$  by using the Bragg law

$$\lambda = 2 d_{hkl} \sin \theta.$$

The lattice strain is defined as

$$\varepsilon_{hkl} = \frac{d_{hkl} - d_0}{d_0}$$

where  $d_0$  is the interplanar distance of the stress-free material. For a detailed treatment of the theoretical bases of this technique and for several relevant examples of application the reader should refer to [2-13].

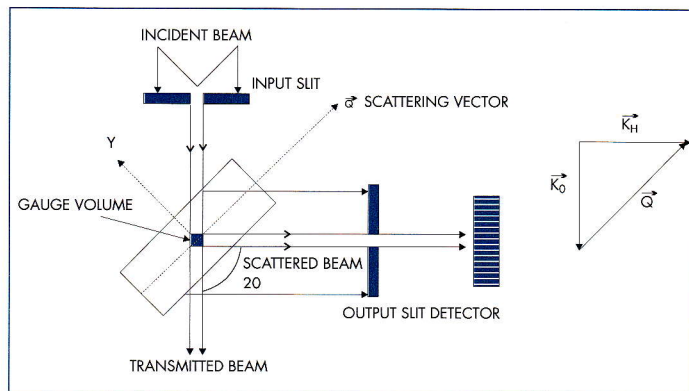


Fig. 1

## EXPERIMENTAL FACILITIES

A strain scanner, installed at the Riso National Laboratory in Denmark [11], allows the simultaneous determination of the strain value in different points of a given component. In the frame of a Brite-Euram project, financed by the European Community, a prototype instrument, ENGIN, dedicated to residual stress measurements, was installed at the world's most intense pulsed neutron source ISIS with a strain resolu-

tion of  $5 \times 10^{-5}$  [7]. Another dedicated instrument (Fig. 2) is under construction at Laboratoire Leon Brillouin, Saclay, in the frame of a French-Italian (INFM) cooperation [14]. A high stress resolution can be obtained by using a double crystal diffractometer as the one installed at the Nuclear Research Center of Rez near Prague [12].

## THE STRESS-FREE REFERENCE SAMPLE

From eq. (2) it appears that in order to determine the strain in a given point of a sample, the knowledge of the interplanar distance  $d_0$  of the stress-free sample is necessary. Each error in  $d_0$  implies systematic errors in the strain value. As a consequence it is necessary to determine  $d_0$  with the highest possible accuracy. Several methods are commonly used to determine  $d_0$ . The most usual one is to measure the interplanar distance on a small sample of the same material submitted to a proper thermal treatment (annealing), in order to relieve any residual stress. A second method consists in measuring the interplanar spacing in a region of the investigated component, which is assumed to be stress-free because unaffected by the process inducing the residual stresses. A third method consists in measuring  $d_0$  in an annealed powder of the investigated material, in which the assumption that the powder

granulates are small enough that the stresses are relaxed, is reinforced by the annealing treatment. A fourth method makes use of the classical condition that the integrals of the stresses and their moments on any sample volume in equilibrium should be zero. In this case the  $d_0$  value is obtained by an iterative procedure.

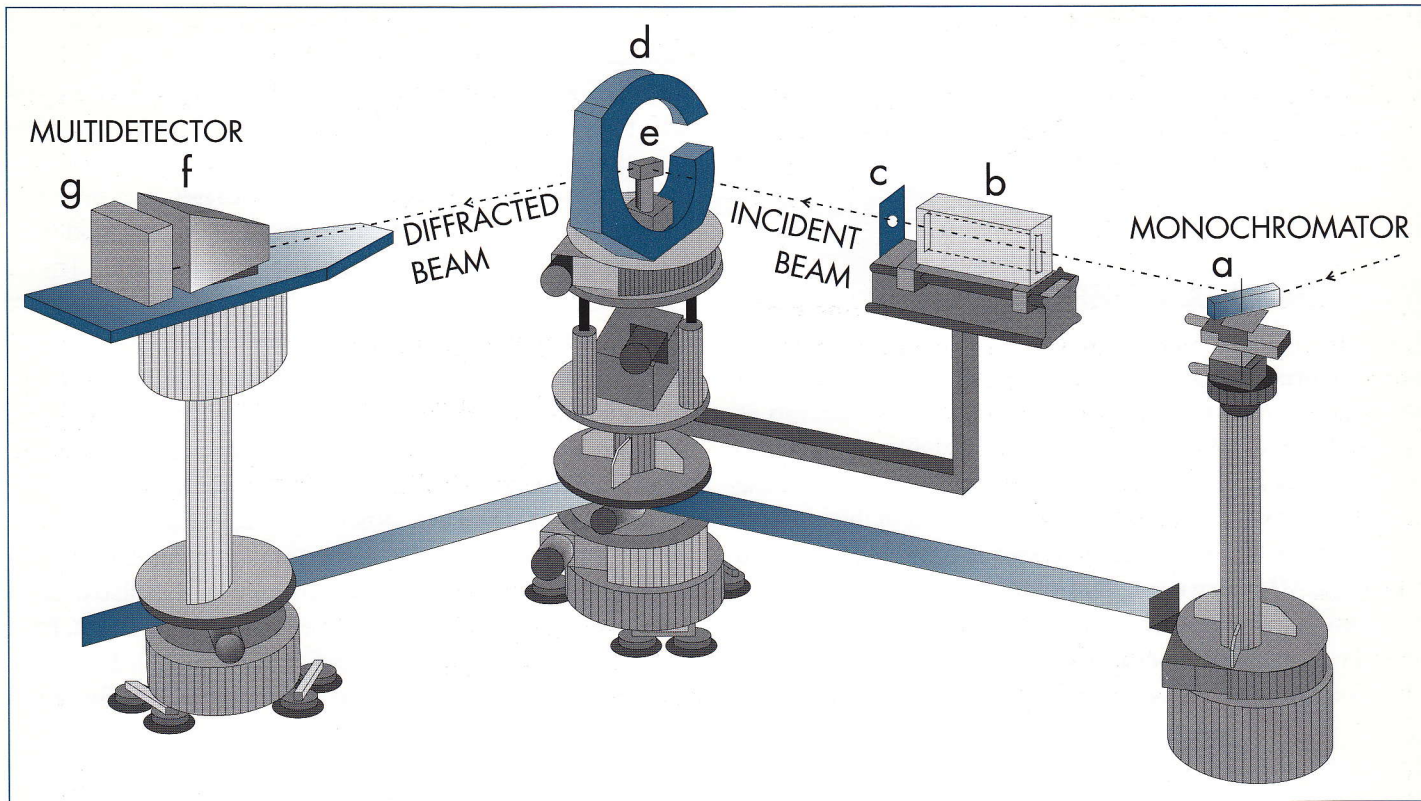


Fig. 4

### STRAIN-STRESS RELATIONSHIP

In the most general case the strains and stresses are triaxial and can be represented by a strain tensor  $\epsilon$  and a stress tensor  $\sigma$ . Fig. 3 shows the axes OXYZ arbitrarily chosen within the sample and a generic direction, defined by the  $\phi$  and  $\psi$  angles, along which the strain  $\epsilon_{\phi\psi}$  is measured, with direction cosines ( $\alpha_1, \alpha_2, \alpha_3$ ) given by

$$\begin{aligned} \alpha_1 &= \sin \psi \cos \phi \\ \alpha_2 &= \sin \psi \sin \phi \\ \alpha_3 &= \cos \psi \end{aligned}$$

The strain  $\epsilon_{\phi\psi}$  is given by

$$\epsilon_{\phi\psi} = \alpha_1^2 \epsilon_{xx} + \alpha_3^2 \epsilon_{zz} + 2 \alpha_1 \alpha_2 \epsilon_{xy} + 2 \alpha_2 \alpha_3 \epsilon_{xy} + 2 \alpha_3 \alpha_1 \epsilon_{zx}$$

This is a linear equation with six unknowns,  $\epsilon_{xx}, \epsilon_{yy}, \epsilon_{zz}, \epsilon_{xy}, \epsilon_{yz}, \epsilon_{zx}$ , which can be exactly solved, in principle, if the strain is measured along six independent directions. However, in practice, the accuracy can be improved if more directions are considered. The simplest directions are along, and at  $45^\circ$  to the axes OX, OY, OZ. After determination of the six unknowns, i.e. of the strain tensor  $\epsilon$ , the principal strain axes OX'Y'Z' and the principal strains  $\epsilon^D$  along them may be found by diagonalisation. Then, if one assumes an elastically isotropic model with Young's modulus E and Poisson's ratio  $\nu$ ,

the principal internal stresses along these axes,  $\sigma_{xx}^D, \sigma_{yy}^D, \sigma_{zz}^D$ , are related to the strains by

$$\sigma_{xx} = \frac{E}{(1+\nu)(1-2\nu)} [(1-\nu) \epsilon_{xx} + \nu (\epsilon_{yy} + \epsilon_{zz})]$$

$$\sigma_{yy} = \frac{E}{(1+\nu)(1-2\nu)} [(1-\nu) \epsilon_{yy} + \nu (\epsilon_{xx} + \epsilon_{zz})]$$

$$\sigma_{zz} = \frac{E}{(1+\nu)(1-2\nu)} [(1-\nu) \epsilon_{zz} + \nu (\epsilon_{yy} + \epsilon_{xx})]$$

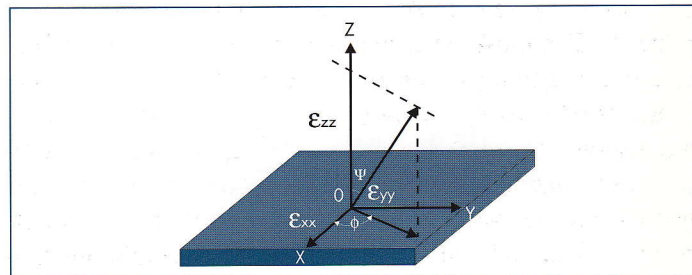


Fig. 5

However one must be careful because in most materials the values of  $E$  and  $\nu$  depend on the lattice planes ( $hkl$ ) used as strain gauge, due to the anisotropy of elastic properties in crystalline materials. As a consequence one should either theoretically evaluate the neutron elastic constants, or better, to

determine them experimentally as it is discussed below in one example concerning residual stress determination in a coating. For a more detailed discussion of this point one should refer to [13].

## METAL MATRIX COMPOSITES

Metal matrix composites (MMC) are of great interest for several industrial applications, like for instance in aircraft or cars technology, due to their reduced weight and advantageous mechanical properties. However before commercial use several improvements must still be done and in this context the determination of residual stresses is of great interest. In fact as the MMC are normally produced at high temperature and there is a difference in the thermal expansion coefficient and elastic constants between fibres and matrix, when they are cooled down to room temperature stresses arise both in

the matrix and in the fibres. Usually the fibres undergo compression along the axis and the matrix expansion along the same direction, as it appears in fig. 4 at room temperature, in the case of a ceramic matrix composite having  $Al_2O_3$  as matrix and SiC as whiskers. When the temperature of the sample is increased the strains (stresses) are progressively relieved as it is expected. Neutron diffraction was also used to determine the strain sharing between matrix and fibres, for a sample subjected to variable external load [15]. Fig. 5 reports the lattice strain measured in the direction of the stress

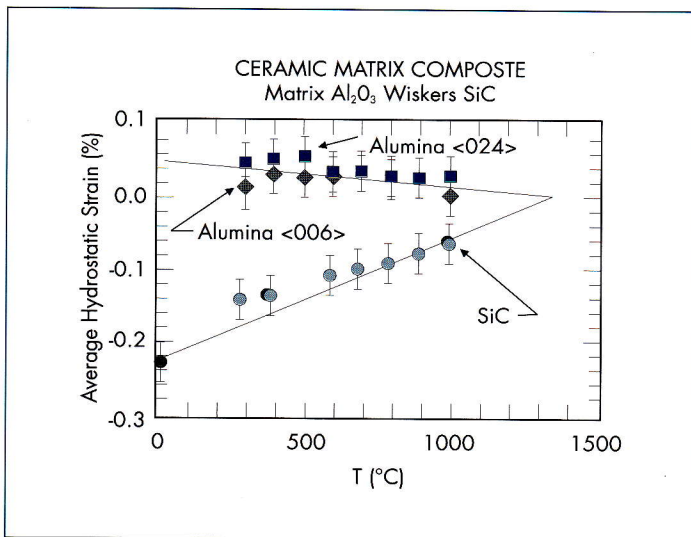


Fig. 4

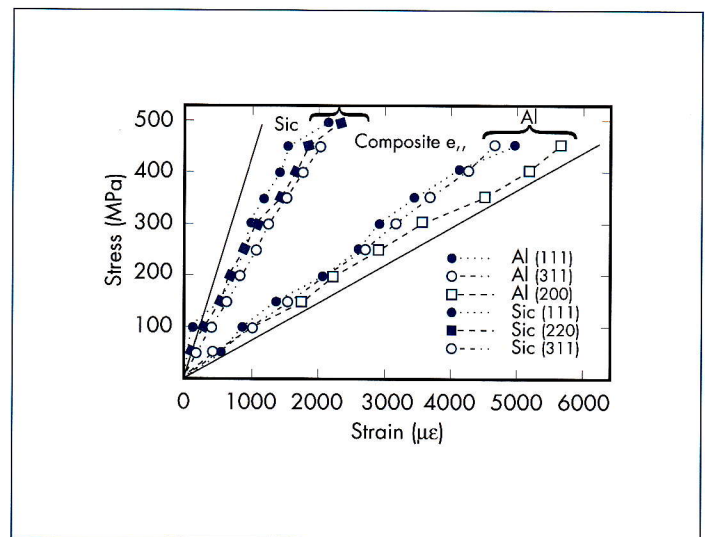


Fig. 5

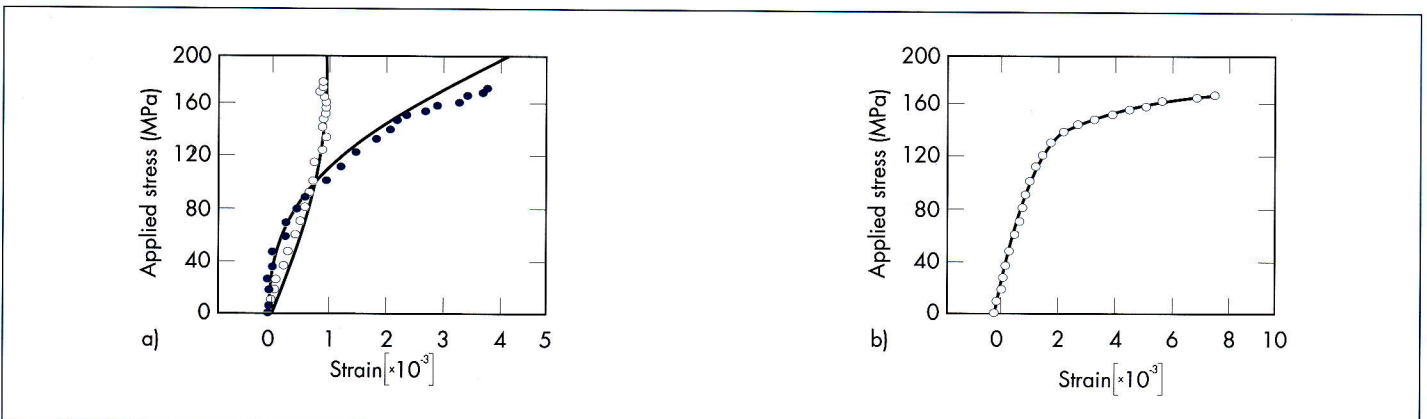


Fig. 6a - 6b

by using three Bragg reflections in each of the (2014) aluminium matrix and the 20% SiC particulate, as a function of the stress. It appears that the deformation in SiC is much smaller than in Al, and that strong anisotropy exists. The solid lines are obtained by theoretical models. A similar experiment was performed on an uniaxial specimen of an aluminum matrix reinforced with 5% in volume of SiC whiskers [5]. Fig. 6a reports the elastic strains, obtained by neutron diffraction, both in the matrix and in the whiskers, as a function of external loading, whereas fig. 6b reports the total macroscopic strain recorded by strain gauges. It appears that for small loads the aluminum is more able to undergo elastic

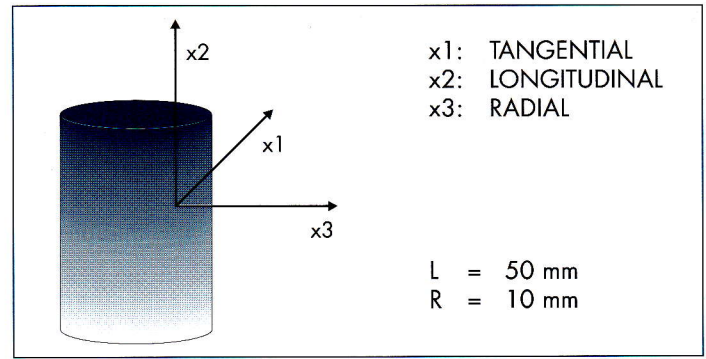


Fig. 7a

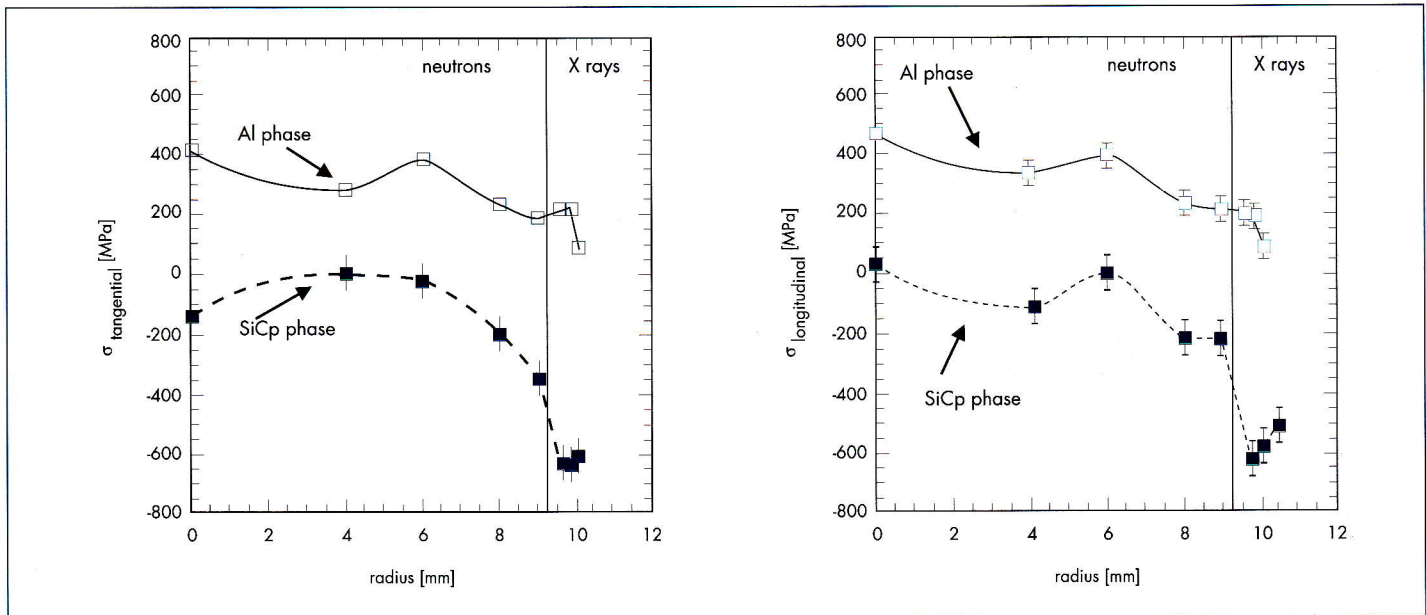


Fig. 7b - 7c

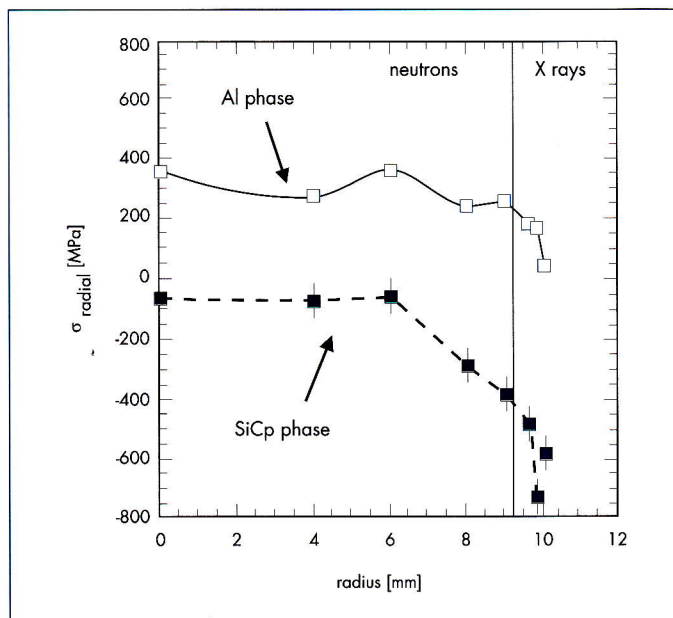


Fig. 7d

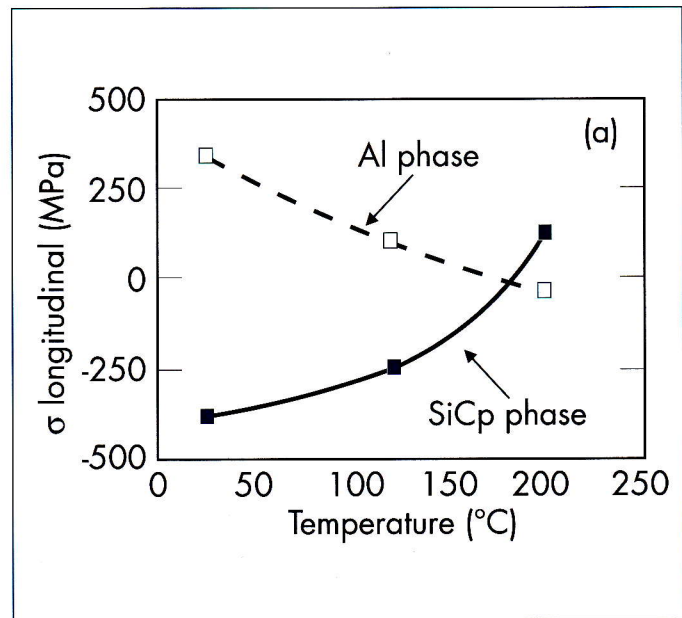


Fig. 8a

deformations, whereas for higher loads the elastic loading is transferred to the SiC. Residual stresses in metal matrix composites (2024 Al alloy matrix reinforced by 25 vol% SiC particulates) were determined by X-ray and neutron diffraction [16]. Both thermal and mechanical residual stresses were considered, by using a four points bending device. Residual stress relaxation was also investigated by neutron *in-situ* measurements. Fig. 7a reports the geometry of the sample, whereas fig.s 7b, 7c, 7d the radial distributions of the residual stresses in the three orthogonal directions shown in fig. 7a. It appears that the matrix is always in a tensile stress state, whereas the reinforcement is in a compressive stress state, as expected by the fact that the thermal expansion coefficient of the matrix is larger than the one of the SiC. Fig. 8a and 8b report the temperature evolutions of longitudinal and transverse stresses, respectively, for the Al matrix and the SiC<sub>p</sub> particulates. As expected the residual stresses are tensile in the matrix and decrease with increasing temperature, becoming compressive at high temperature while an opposite behaviour is observed for the SiC<sub>p</sub> particulates.

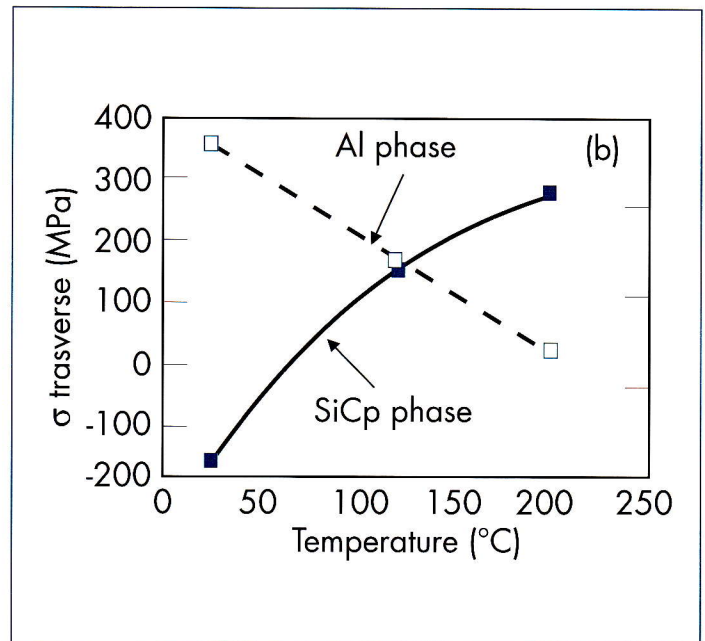


Fig. 8b

## WELDS

During the welding process very strong temperature gradients occur, which induce very high residual stresses, sometimes of the order of magnitude of the yield stress. It is therefore of great interest to determine experimentally these stresses and the eventual relief after thermal treatments, as calculations procedures, like the ones based on finite elements, are reliable only in the most simple cases. The neutron diffraction technique was largely used to investigate the strain profiles close to welds. Only few example are reported here.

### Double - V weldments

Fig. 9 reports the residual stress profiles through a double - V weldment sample (50 D C-Mn steel) as determined by using the (211) neutron Bragg reflection [3]. The points refer to the stress values along the y and z directions determined, by using  $E = 207$  GPa and  $\nu = 0.28$ , as a function of the z coordinate. The shaded area refers to data obtained by a conventional destructive method. The agreement is quite satisfactory.

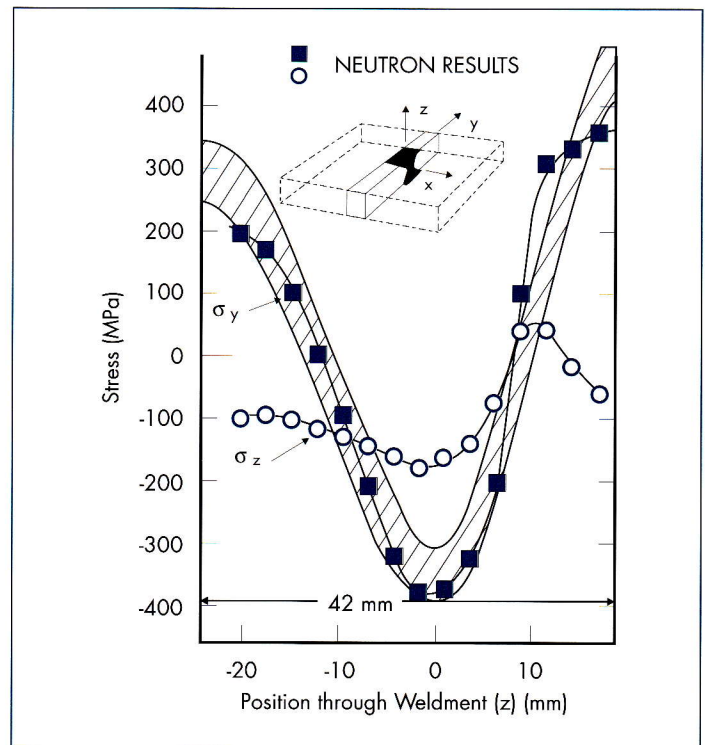


Fig. 9

### T - weldment

Fig. 10a shows the geometry of an experiment, where by using a Position Sensitive Detector (PSD) it was possible to record simultaneously the strain in 34 points (fig. 10b) along the incident beam [11]. Several scans were

obtained at different distances from the welded area, by shifting the T-butt weld along the z axis. Four of them are reported in fig. 10b. It appears that the welding process can induce very high residual strains (stresses) until an appreciable fraction of the materials yield strength.

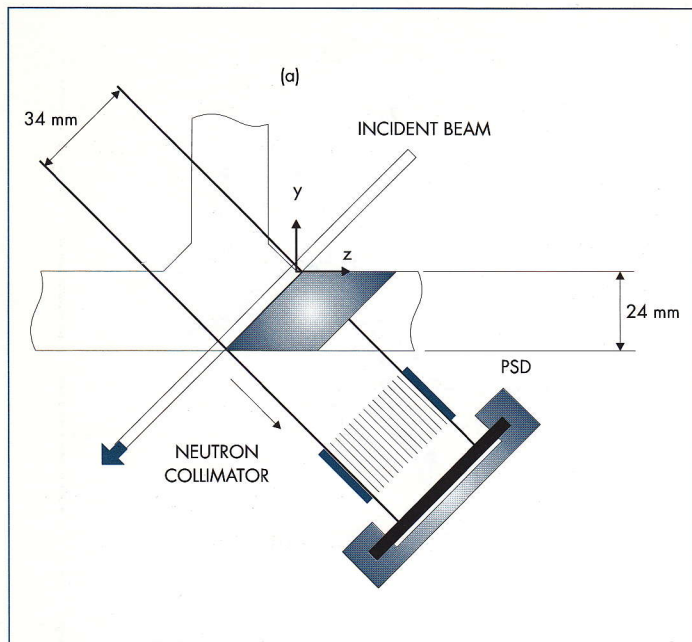


Fig. 10a

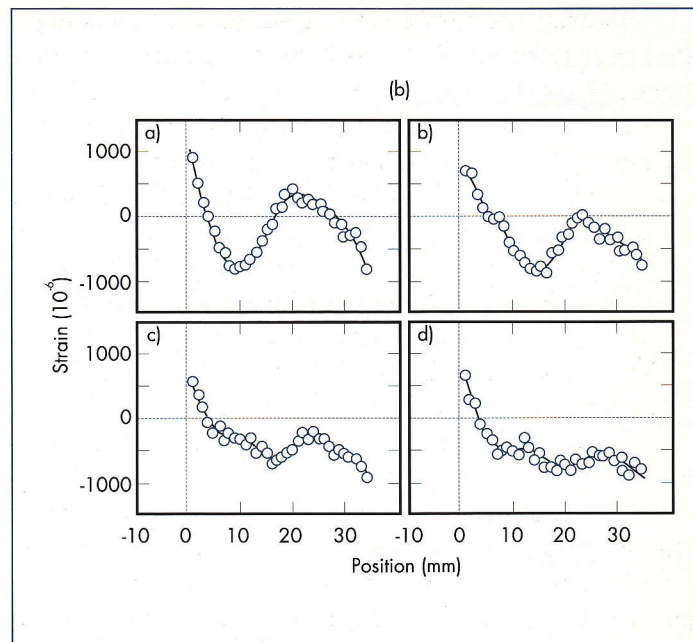


Fig. 10b

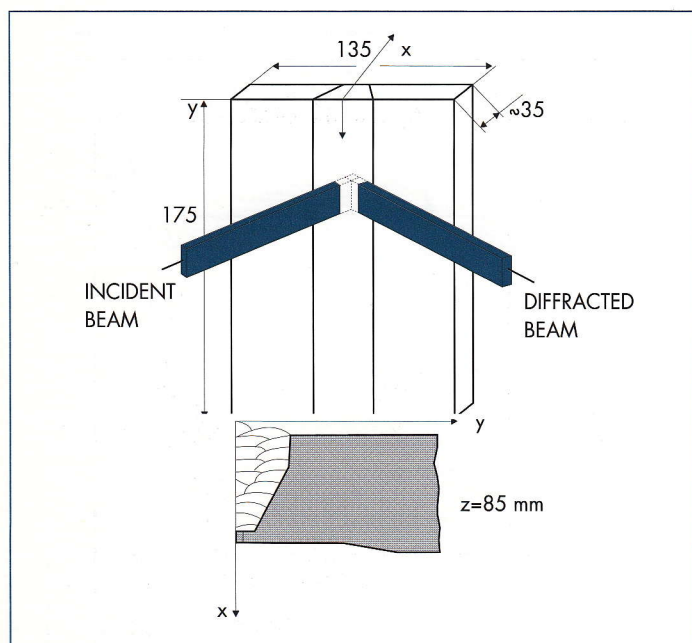


Fig. 11a

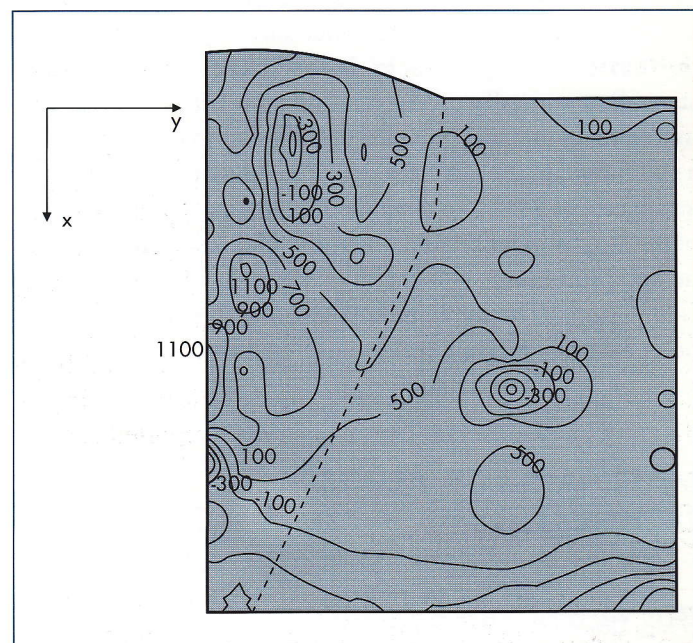


Fig. 11b

## V - weldments

A recent experiment was performed on a weld of AISI 304 stainless steel [17]. Fig. 11a shows the weld geometry and the geometry of the neutron diffraction experiment including the definition of the probe element of dimensions  $2.5 \times 2.5 \times 20 \text{ mm}^3$ . The (111) reflection was used to determine a map of the strain which is reported in fig. 11b. A strong strain gradient appears in the weld region itself. This figure shows the

advantage of neutrons as compared to X-rays. The use of the second technique would have led to an information concerning few hundreds micrometers beneath each surface, with a consequent lack of information on the strains inside the bulk.

## COMPARISON BETWEEN FINITE ELEMENT CALCULATIONS AND NEUTRON DIFFRACTION DATA

One of the most peculiar advantages of the residual strain measurement technique by neutron diffraction is that it can be applied in the bulk of the engineering components and can be therefore compared with the stresses or strains calculated by finite element method, and so used to validate the different codes. Several examples of this kind exist in the literature and some comparisons will be occasionally presented in the sections below.

### THICK WALLED TUBES

Thick walled tubes are used in many industrial plants and are often submitted to variable internal pressures. In order to increase the fatigue life it is suitable to provide the tube before use with a residual stress field of compressive nature in tangential direction near the inner surface in order to delay the starting of fatigue cracks. In this frame a tube of a CrMo steel alloy normally used in marine diesel engines, was submitted to an internal pressure of 2500 bar in order to induce a strain field in the material [11]. Fig. 2 reports the schematic arrangement used to determine the profile through the tube of the strains in tangential direction. The results are reported in fig. 12 in comparison with predictions of finite element calculations. The agreement is good with exception of the outer surface, where a certain discrepancy exists.

## MATERIALS FOR AEROSPACE TECHNOLOGY

### Gas turbine components

Residual stresses in aeroengine compressors arise as a result of machining operations and welding together of the individual disks. In order to counteract the negative influence of these residual stresses, it is often convenient, in order to increase the life of the component, to induce expressly proper residual stresses by using, for instance, the shot-peening technique [18]. Compressive stresses are induced into the surface of components by this method. Fig. 13 shows how shot peening can strongly increase the fatigue performances of a nickel superalloy. Fig. 14 shows the geometry of a neutron diffraction experiment. Fig. 15 reports the obtained residual stress field through a 12.75 mm thick plate, having a bulk elastic modulus of 220 GPa and yield strength of 1200 MPa.

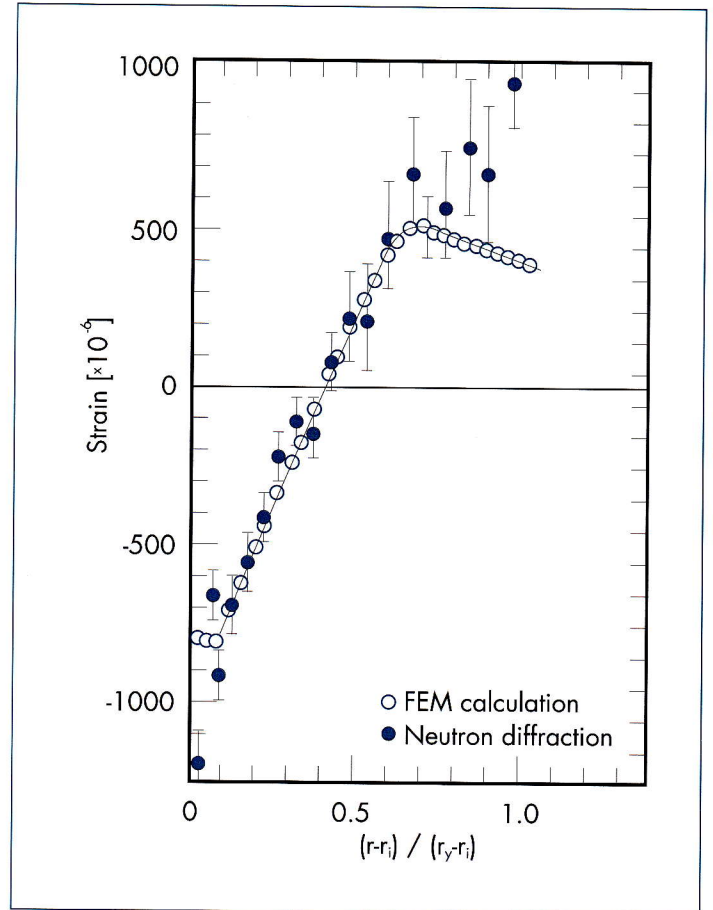


Fig. 12

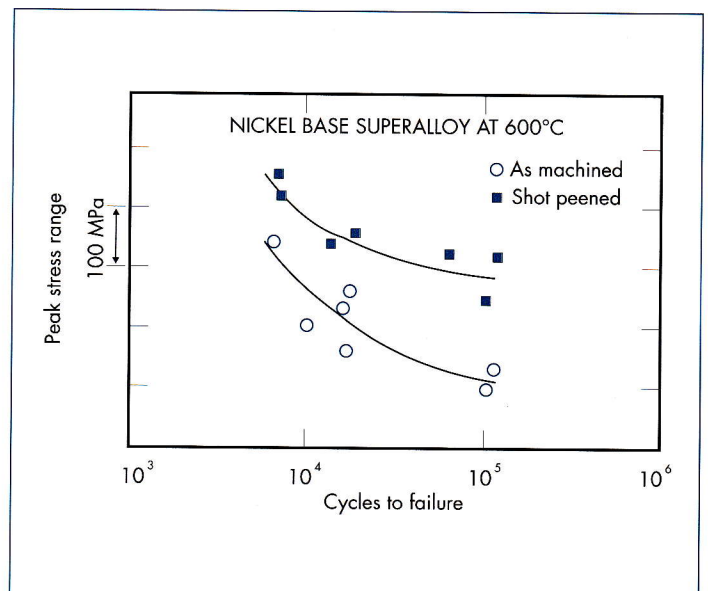
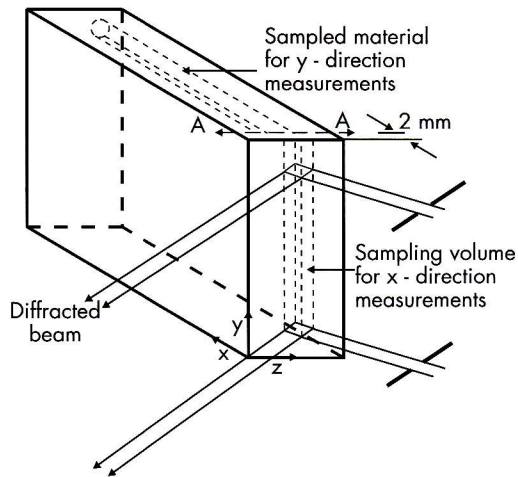


Fig. 13



**Sample moves incrementally along line A-A to allow the sampling volume to traverse the entire specimen. A-A is at  $x = 2$  mm**

**INPUT MASKS**

- 1 mm wide for plate 1  
0.5 mm wide for plate 2
- 20 mm high

Fig. 14

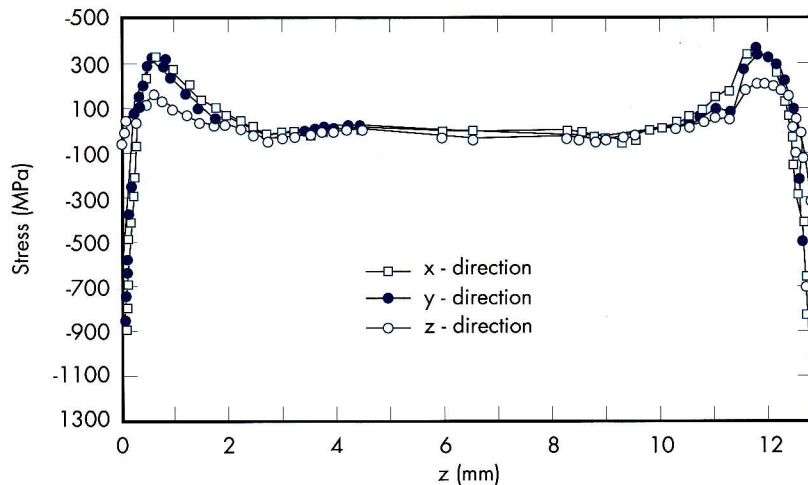


Fig. 15

Compressive stresses are observed at surfaces, and tensile stress peaks at a depth less than a millimeter. Moreover Bragg peak broadening observations suggest that the depth of plastic deformation caused by the peening was no greater than about 0.5 mm.

**Cold expanded holes**

Cold expansion technique is widely used in aerospace industry in order to counteract the fatigue process near the edge of boreholes with a consequent enhancement of the fatigue life. The expansion is obtained by insertion of a hard tool having a larger diameter as compared to the initial one of the hole. After the treatment and removal of the tool, the hole edge is plastically deformed and shows compressive residual stresses. Fig. 16 reports the residual stress distribution around a cold

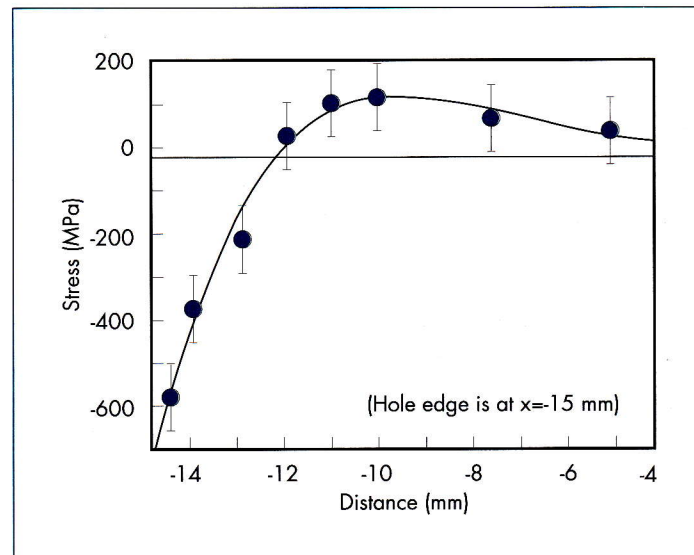


Fig. 16

expanded hole by 4% in a mild steel specimen, where the initial diameter was 9.52 mm [19]. The data were obtained at the ENGIN prototype by fitting the (110) reflection in a time

of flight experiment. An appreciable compressive stress is observed.

## MATERIALS FOR FUSION REACTOR TECHNOLOGY

The "first wall" of a thermonuclear fusion reactor is one of the most critical components as it is exposed to fluxes of different radiations like high energy neutrons and ions, electromagnetic radiation, and to thermo-mechanical stresses associated with the pulsed nature of the reactor. In order to simulate these stresses an AISI 316 steel mock-up of the first wall was submitted to 27000 thermal cycles of 5 mHz, with a thermal flux varying from 0 to 500 kW/m<sup>2</sup>. A neutron diffraction experiment [20] was performed in order to determine the residual strains in the component after the treatment. The geometry of the experiment is reported in fig. 17. The Bragg diffraction from {111} planes was used, by choosing the neutron wavelength in order to have  $2\theta_B = 90^\circ$ . The gauge volume was  $1.3 \times 1.3 \times 30 \text{ mm}^3$ . The reference interplanar distance  $D_{111} = 0.20686(3) \text{ nm}$  was determined by diffraction from an unstrained piece of the same material. By differentiation of the Bragg, law one obtains the strain  $\epsilon$  as

$$\epsilon = \frac{\Delta D}{D} = \cotg \theta \cdot \Delta \theta$$

Moreover it was above reported that the strain  $\epsilon_{\varphi\psi}$  in the direction of the exchanged momentum  $Q_{\varphi\psi}$  (see fig. 17) can be expressed by eq. 4. The measurements were performed at  $Q = 0$  and it was assumed that the strain does not depend from  $y$ . The two-dimensional strain distribution in the  $(x, z)$  plane is then obtained from eq.s 3 and 4.

$$\epsilon_{\varphi\psi} = \epsilon_{\psi} = \sin^2 \psi (\epsilon_{xx} - \epsilon_{zz}) + \epsilon_{xz} \sin(2\psi) + \epsilon_{zz}$$

By measuring the  $\epsilon$  values as a function of  $\sin^2 \psi$ , one should obtain an ellipse. Actually straight lines were obtained, in any case, with the consequence that  $\epsilon_{xz}$  should be equal to zero. Moreover  $\epsilon(0) = \epsilon_{zz}$  and  $\epsilon(1) = \epsilon_{xx}$  represents the strains in direction parallel and perpendicular to the surface, respectively (see fig. 17). Fig. 18 reports the measured values of  $\epsilon_{xx}$  and  $\epsilon_{zz}$  as functions of depth along a line from surface to central hole axis, in comparison with the results of calculations based on the finite element technique: the agreement appears to be quite satisfactory. Another experiment performed on a brazed graphite/molybdenum sample of interest for fusion technology will be presented below [28].

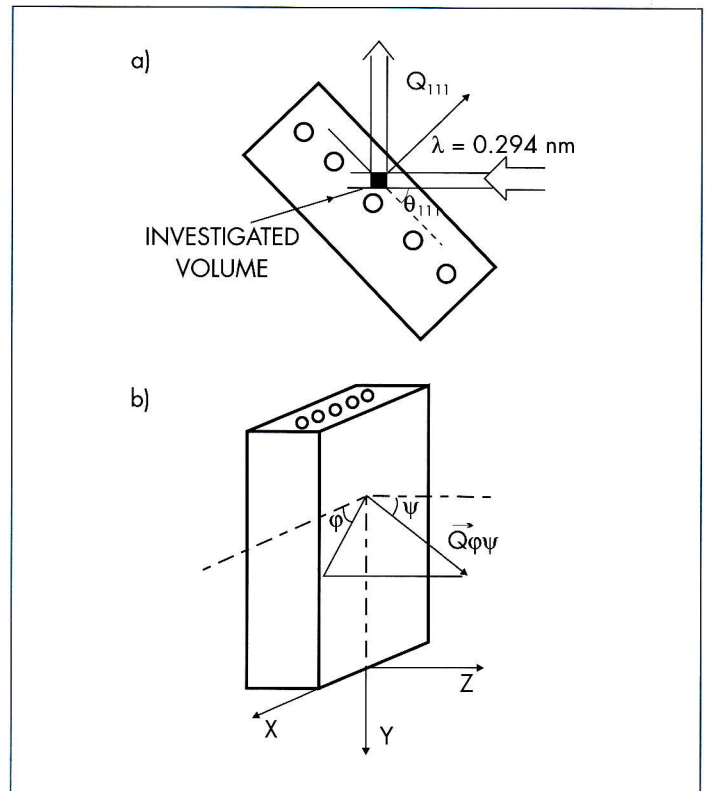


Fig. 17

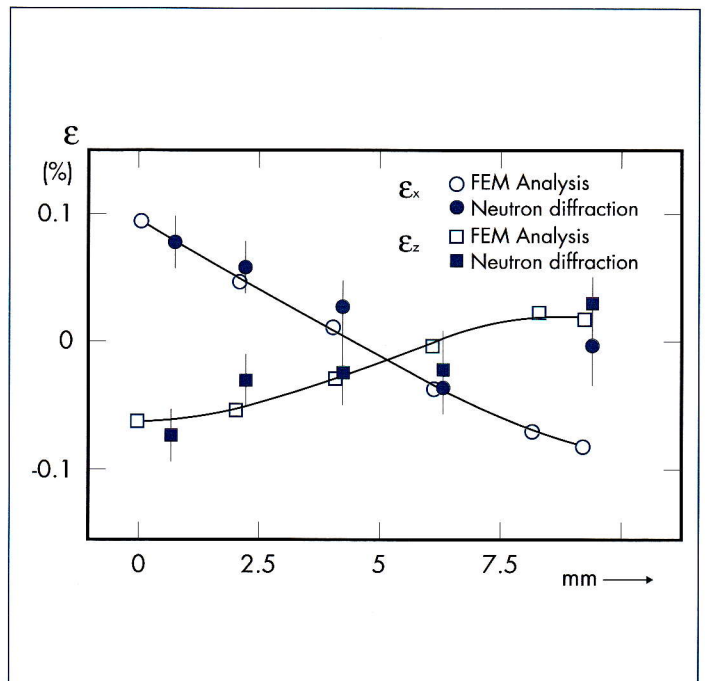


Fig. 18

## RAILWAY RAILS

Residual stresses were measured by neutron diffraction on railway rails [21-22]. The manufacturing process induces residual stresses in railway rails as a consequence of differential cooling rates, which induce plastic deformation, and of subsequent hot rolling and thermal treatments. Moreover during the service period the trains induce additional plastic

components. The figure reports the longitudinal stresses in the two components and confirms the prediction that they are practically relaxed in the slice and present strong variations in the plate: there is tension in the foot and in the head and compression in the web as well as in a thin layer on the top which is submitted to a compressive load by the passing trains.

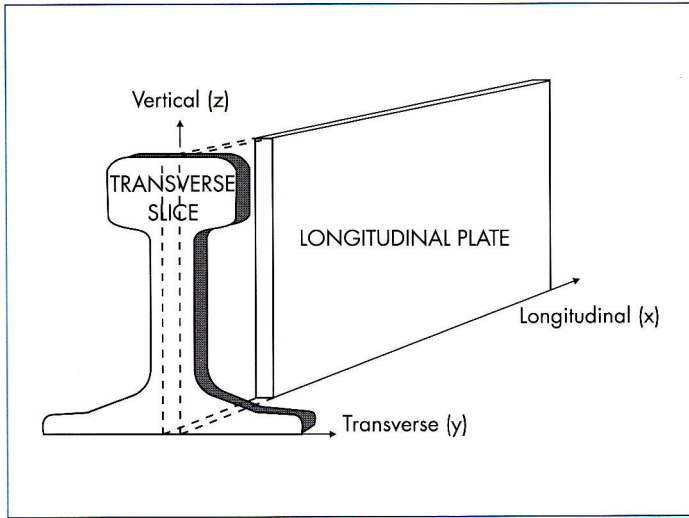


Fig. 19

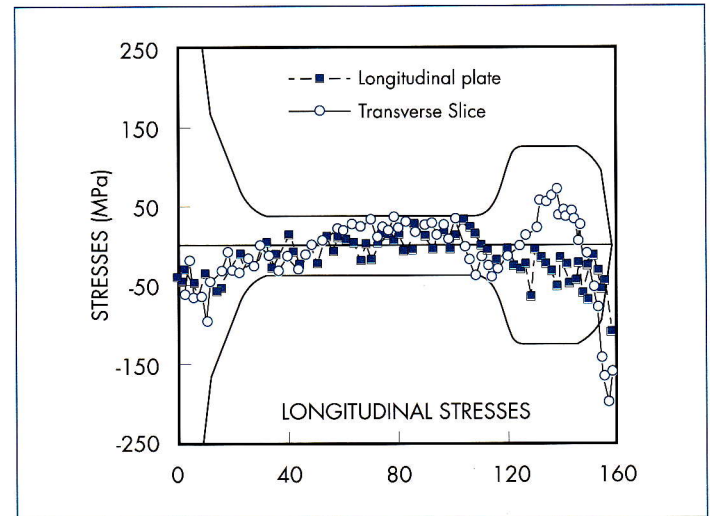


Fig. 20

deformations. The engineers need to know the residual stresses in the rails, as they can lead to fatigue failures and in extreme cases to fracture and train derailment. Ref. [21] reports results of neutron diffraction measurements on a transverse slice and longitudinal plate samples cut from a railway rail (fig. 22). Fig. 20 reports the residual stresses deduced from neutron diffraction in transverse and longitudinal sections cut from a used railway rail: the measurements were done along the centre line of the two 10 mm thick and 160 mm high

Ref. [21] reports also transverses and vertical stresses in both the plate and the slice. Fig. 21 shows the stress contours obtained in the head of a slice of a used railway rail, both for the transverse and vertical direction [22]. Compressive stresses are observed in an area below the running surface and tensions below this area. Moreover asymmetries and strong stress gradients are observed. This data should be helpful in explaining failures in the track due to rolling contact fatigue.

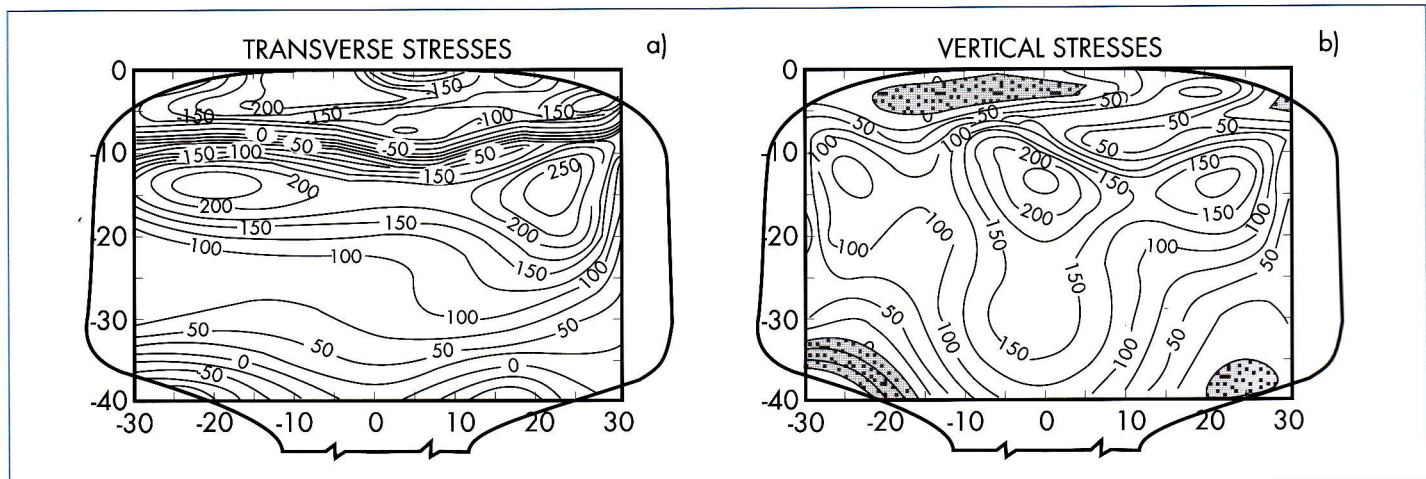


Fig. 21

## BRAZED COMPONENTS

Brazed ceramic-steel components are of great interest in technology, because on one hand ceramics have great advantages as hardness, resistance to wear, corrosion, high working temperatures and low thermal conductivity, but, on the other hand, they have some disadvantages (compensated by the high ductility of steels) as they are brittle and therefore have low resistance to impact loading and tensile stresses. One problem associated to these components is given by the residual stresses arising in the two materials when they are cooled from the brazing temperature, as a consequence of their different thermal properties. An experimental and theoretical investigation of the residual stress distribution in brazed ceramic-steel components is reported in ref. 23. Fig. 22a reports the scheme

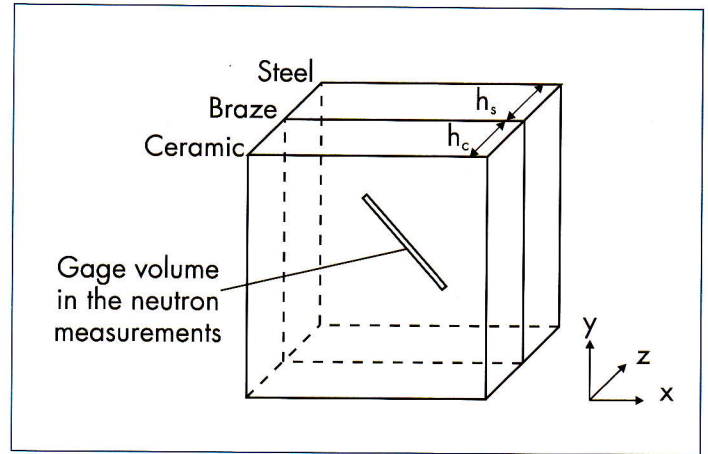


Fig. 22a

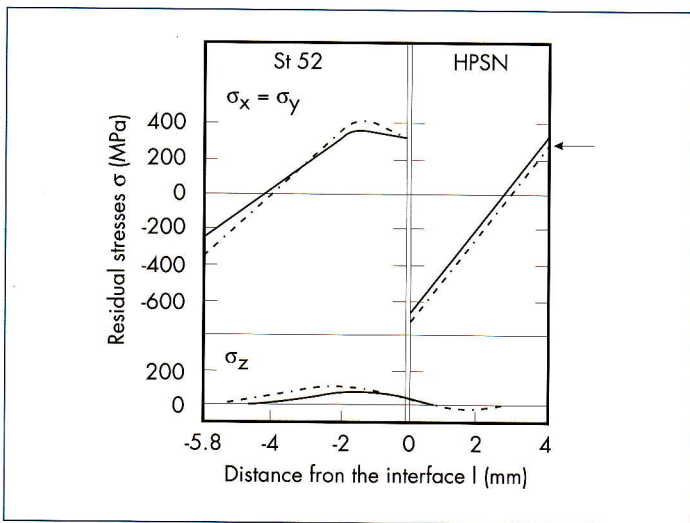


Fig. 22b

of the samples. The steel was either a plain carbon steel (German grade Ck45, 0.45 wt. % C) or an unalloyed steel (German grade St 52, 0.2 wt. % C, 1.5 wt. % Mn). Two kinds of ceramics were used: hot pressed  $\text{Si}_3\text{N}_4$  and  $\text{ZrO}_2$  with 3 mol. %  $\text{Y}_2\text{O}_3$  to stabilize the tetragonal phase. The thickness of the ceramic plates was  $h_c = 4$  mm, whereas the one of the steel plates was varying from 3.7 mm till 10 mm. AgCuTi with composition 70.5% - 26.5% - 3% was used as the braze alloy. The thickness of the braze gap was 0.1 - 0.2 mm and the braze temperature was  $950^\circ\text{C}$ . Fig. 22b reports a typical stress distribution across the specimen. The two arrows indicate the results of similar measurements by X-ray diffraction. The continuous lines are the experimental results, whereas the broken lines are the results of finite element calculations based on the temperature dependent elastic-plastic properties of the materials. At the interface a stress of tensile nature is observed in the steel and of compressive nature in the ceramic. Moreover, whereas the residual stress distribution in the ceramic is almost linear, non-linearity is observed in the steel,

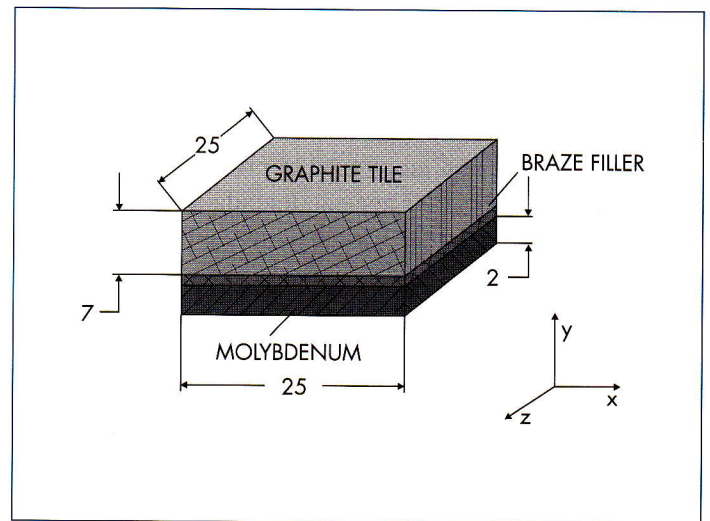


Fig. 23a

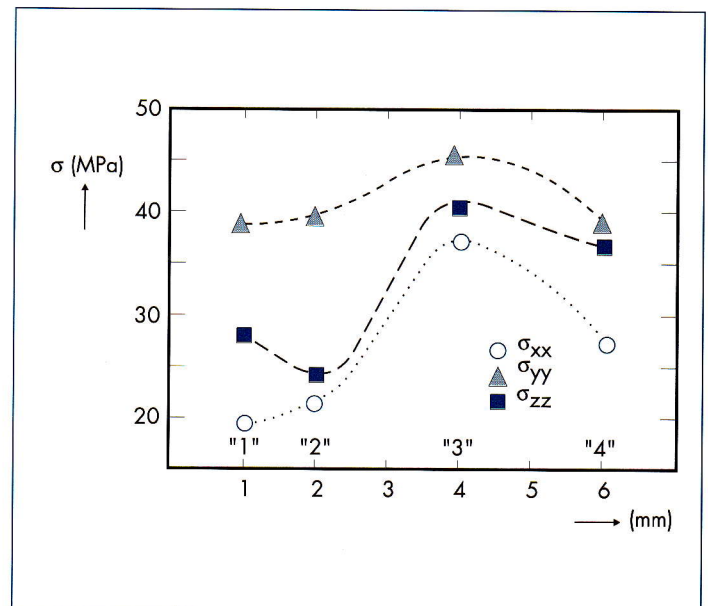


Fig. 23b

indicating plastic deformation [24], which is confirmed by calculations. A good agreement is observed in general between the finite element calculations and the neutron and X-ray data. Neutron diffraction was also used to investigate the stress field remaining after brazing at 860°C, in graphite/molybdenum samples of interest for fusion reactor technology [25]. The sample was a mock-up of a metallic cooling

tube surrounded by an armor, to be used in connection with the divertor component of near-term prototype fusion reactors, such as NET/ITER. More specifically, the tube material was molybdenum, whereas the armor material was graphite [26]. Fig. 23a reports the geometry of the investigated sample, whereas fig. 23b the stresses in the three main directions as a function of the distance from the brazing plane.

## METAL ADHESIVE JOINTS

The feasibility of the determination by neutron diffraction of stress fields near the metal-adhesive interface was demonstrated on an aluminium alloy assembled by a single component epoxy adhesive [27]. The specimen was submitted to a

macroscopic strain by using a special set-up. The obtained results were compared with theoretical predictions based on finite element calculations.

## COATINGS

Coatings are more and more used to protect the surface of technological components against degradation processes of chemical nature, such as oxidation, corrosion and erosion or of mechanical nature such as wear and fretting. Very often residual stresses arise in the coatings due to the different thermal properties of the two materials, which can produce delamination. Neutron diffraction can be used in order to determine the stress profiles from the coating surface to the substrate through the interface. An example can be found in ref. [28], where a ferritic steel cylinder, of diameter  $\phi = 78$  mm, remetalled by Plasma semi-Transferred Arc with 2 mm martensitic stainless steel, was investigated. Other usual techniques of coatings deposition are the combustion flame, arc wire, high velocity combustion and plasma spraying: this last technique is used in particular in dental and orthopaedic prosthesis. As the deposition process might introduce a considerable texture in the coating, it was necessary to experimentally determine the neutron Diffraction Elastic Constants (DEC) for both the substrate and the coating. In fact the theoretically evaluated DEC not always are reliable. The DEC are defined as

$$\left(\frac{1}{2}S_2\right)_{hkl} = \frac{1 + \nu_{hkl}}{E_{hkl}}$$

$$(S_1)_{hkl} = -\frac{\nu_{hkl}}{E_{hkl}}$$

where  $\nu_{hkl}$  and  $E_{hkl}$  are the Poisson's ratio and the Young's modulus, respectively, referred to the diffraction plane hkl, which in the considered case was (200). The DEC were obtained by applying an uniaxial stress ( $\sigma_{xx} = \sigma_{app}$ ). The equation used [31] is

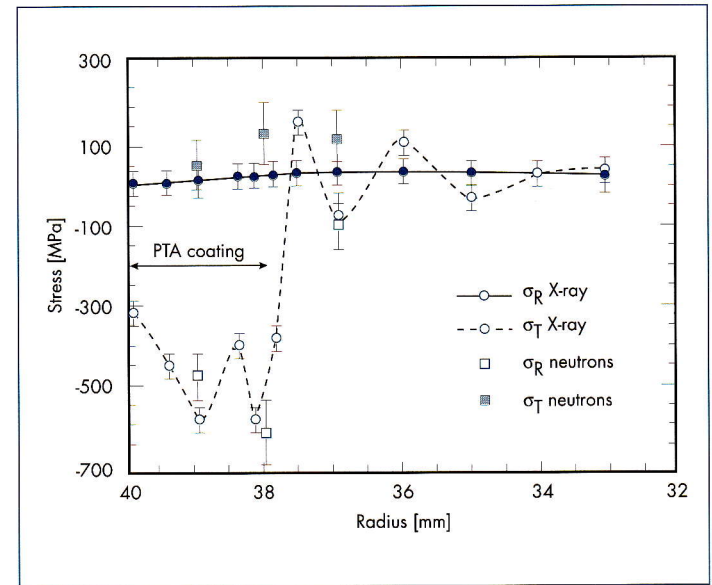


Fig. 24

$$\epsilon_{\psi} = \left(\frac{1}{2}S_2\right)_{hkl} \sigma_{xx} \sin^2 \psi + (S_1)_{hkl} (\sigma_{xx} + \sigma_{yy})$$

where  $\psi$  is the angle between the sample normal and the direction of the scattering vector  $Q$ . By measuring  $\epsilon_{\psi}$  as a function of  $\sin^2 \psi$ , for a fixed value of  $\sigma_{app}$ , it is possible to obtain the parameter  $\alpha$ , given by

$$\alpha = \frac{\partial \epsilon_{\psi}}{\partial (\sin^2 \psi)} = \left(\frac{1}{2}S_2\right)_{hkl} \sigma_{app}$$

and also the value  $\epsilon_{\psi=0}$  as a function of  $\sigma_{app}$ . The neutron Diffraction Elastic Constants are obtained by partial differentiation of eq. 12 and using eq. 11, written for  $\psi = 0$

$$\left(\frac{1}{2}S_2\right)_{hkl} = \frac{\partial \alpha}{\partial \sigma_{app}} \quad (S_1)_{hkl} = \frac{\partial (\epsilon_{\psi=0})}{\partial \sigma_{app}} = \frac{\partial \beta}{\partial \sigma_{app}}$$

where  $\beta = \varepsilon_{v=0}$ . The elastic constants were measured with respect to the three principal directions and were used to evaluate the residual stresses in the sample, from the measured strains. Fig. 24 reports the distributions along the sample radius of the radial ( $\sigma_r$ ) and tangential ( $\sigma_t$ ) stresses in comparison with the results of a similar experiment by X-ray

diffraction, in which the residual stresses at different depths were obtained by successive chemical polishing, after correction for the layer removal. Strong compressive tangential stresses are observed in the coating, with a drastic change at the interface. On the other hand the radial stresses are tensile and almost constant through the interface.

## FATIGUE CRACKED SAMPLES

### Stress field during fatigue cycling of a cracked test specimen

The triaxial stress field along the center line of cracking of a compact fatigue test specimen of ferritic steel, BS 4360, was determined by neutron diffraction [29]. The specimen had overall dimensions of ~ 31 mm high, 49 mm along the crack direction and 13 mm thick. The specimen was subjected to 20,000 cycles of a tensile stress with an intensity varying between a minimum of  $K = 3$  and a maximum of  $K = 34$  MPa mm<sup>1/2</sup>, so that a crack of ~ 3 mm length formed from the notch. The cycling was stopped at the maximum level, and the bolt screwed in place in order to keep constant the stress level during stage I of the measurements, whereas it was removed during the stage II. The obtained stress field during stage I is reported in fig. 25. Further details on the experiment can be found in ref. [29], together with a discussion in terms of theoretical predictions based on fracture mechanics calculations.

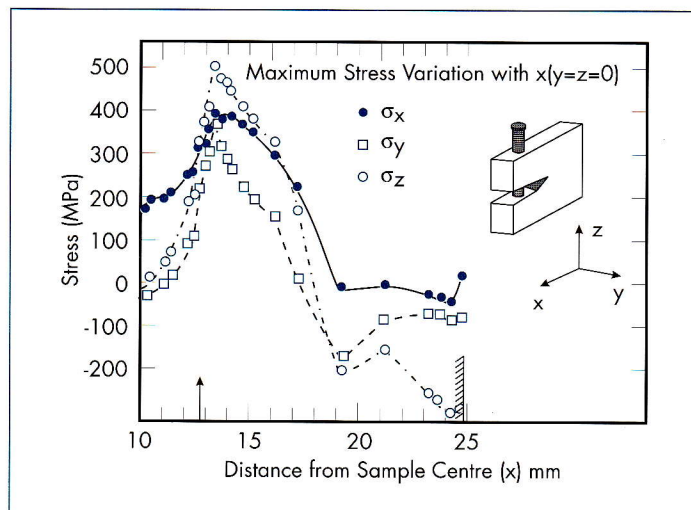


Fig. 25

## INVESTIGATION OF LARGE GRAINED SAMPLES

The analysis of residual stresses in large grained materials was performed both theoretically and experimentally by using X-ray and neutron diffraction [30] [31]. The recording of the neutron diffraction by single crystallites was possible by using fine collimators and diagrams. In particular inhomogeneous elastic and plastic deformation behaviours of crystallites were analyzed by applying different external loads. Appreciable variations from grain to grain were obtained. Moreover by comparing the deformation distributions observed in grain clusters with the deformation states calculated for free single crystals, the extent of the crystallite-crystallite interaction in the polycrystals was obtained.

## CONCLUSIONS

Several examples were presented of non destructive stress determination inside the bulk of materials and components by using neutron diffraction. This technique, which is unique in providing such kind of information, is going to increase its capabilities, as far as new dedicated instruments are being built at different neutron source, in parallel to the adoption of multidetector system and to the increase of both spatial and stress resolution. In conclusion this method of stress determination will be more and more useful not only in several problems of interest for material science but also for direct applications in a progressively larger number of technological domains.

## ACKNOWLEDGEMENTS

It is a pleasure to thank Miss Simona Franguelli for typing the manuscript and Mr. Sirio Polenta for the drawings preparations.

## REFERENCES

- [1] Rustichelli, F., *Met. Sci. and Techn.*, 11 (1993), 118.
- [2] Proceedings of the NATO Advanced Research Workshop on Measurement of Residual and Applied Stress Using Neutron Diffraction (Oxford, March 18-22, 1991) M.T. Hutchings, A.D. Krawitz Eds., Kluwer Academic Publishers (1992).
- [3] Allen, A.J., M.T. Hutchings, C.G. Windsor, C. Andreani, *Advances in Physics*, 34 (1985), 445.
- [4] Priesmeyer, H.G., J. Larsen, D. Meggers, *J. Neutron Research*, 2 (1994), 31.
- [5] Lorentzen, T., *J. of Neutr. Res.*, 1 (1993) 13.
- [6] Edwards, L., M.W. Johnson, H.G. Priesmeyer, F. Rustichelli, P.J. Withers, J. S. Wright, "Precise measurements of internal stresses within materials using neutrons", in "Residual Stresses" eds. Hauk, V., H.P. Hovgard, E. Macherauch, H.D. Tietz, Proc. 3rd Europ. Conf. on Residual Stresses, Publ. DGM, Oberursel, FRG, (1993) 323.
- [7] Withers, P.J., I.B. Harris, L. Edwards, D.Q. Wang, M.W. Johnson, J.S. Wright, H.G. Priesmeyer, J. Larsen, J.A. Goldstone, F. Rustichelli, G. Albertini, Proceedings of the International Symposium on Advanced Materials for Light Weight Structures (Noordwijk, Nederlands '94).
- [8] Pintschovius, L., V. Jung, *Mat. Sci. and Engn.*, 61 (1983), 455.
- [9] Holden, T.M., J.H. Root, V. Fidleris, R.A. Holt, G. Roy, *Mat. Sci. Forum*, 27/28 (1988), 359.
- [10] Albertini, G., F. Carsughi, R. Coppola, D. D'Angelo, Proc. of Int. School of Physics "Enrico Fermi" Course CXIV, Industrial and Technological Applications of Neutrons (Lerici, June 19-29, 1990) M. Fontana, F. Rustichelli and R. Coppola Eds., North Holland (1992) p. 145.
- [11] Juul Jensen, D., T. Lorentzen, Proc. of Int. School of Physics "Enrico Fermi" Course CXIV, Industrial and Technological Applications of Neutrons (Lerici, June 1929, 1990) M. Fontana, F. Rustichelli and R. Coppola Eds., North Holland (1992) p. 201.
- [12] Vrana, M., P. Lukas, P. Mikula, J. Kulda, *Nucl. Instr. and Meth. in Phys. Res.*, A338 (1994), 125.
- [13] Hutchings, M.T., p. 3 of ref. [2].
- [14] Ceretti, M., R. Coppola, A. Lodini, M. Perrin, F. Rustichelli, *Physica*, in print.
- [15] Hutchings, M.T., *Nondestr. Test. Eval.* 5 (1990) 395.
- [16] Ceretti, M., M. Kocsis, A. Lodini, *Science and Engineering of Composite Materials*, in print.
- [17] Albertini, G., M. Ceretti, R. Coppola, S. Ghia, A. Lodini, P. Mariani, M. Perrin, F. Rustichelli, *Met. Sci. and Techn.* 11 (1) (1993) 18.
- [18] Ezeilo, A.N., P.S. Webster, G.A. Webster, P.J. Webster, p. 535 of ref. [2].
- [19] Edwards, L., D.Q. Wang, M.W. Johnson, J.S. Wright, H.G. Priesmeyer, F. Rustichelli, G. Albertini, P.J. Withers, I.B. Harris, Proceedings of the International Conference on Residual Stresses, Baltimore 8-10 June 1994, p. 220.
- [20] Albertini, G., G. André, R. Matera, P. Miele, P. Merola, M. Perrin, F. Rustichelli, *Mat. Sci. and Engn.* A148 (1991) 211.
- [21] Webster, P.J., X. Wang, G. Mills, p. 517 of ref. [2].
- [22] Webster, G.A., p. 21 of ref. [2].
- [23] Pintschovius, L., N. Pyka, R. Kusjmaul, D. Munz, B. Eigenmann, B. Scholtes, *Mat. Sci. and Engn.* A177 (1994) 55.
- [24] Iancu, O.T., D. Munz, B. Eigenmann, B. Scholtes, E. Macherauch, *J. Am. Ceram. Soc.* 73 (1990) 1144.
- [25] Ceretti, M., R. Coppola, E. Di Pietro, A. Lodini, M. Perrin, A. Piant, F. Rustichelli, *J. of Nucl. Mat.*, 212-215 (1994) 1617.
- [26] Cardella, A., E. Di Pietro, M. Brossa, U. Guerreschi, M. Reale, N. Reheis, G. Vieider, *Fusion Technology 1992*, Proceedings of 17th S.O.F.T. Rome, Sept. 1992. C. Ferro, M. Gasparotto and H. Knoepfel Ed.s., North Holland (1993) p. 211.
- [27] Li, J., M. Perrin, M. Ceretti, F. Dunstetter, A. Lodini, *Memoires et Etudes Scientifiques Revue de Metallurgie*, Fevrier 1992, P. 115.
- [28] Ceretti, M., H. Michaud, M. Perrin, A. Lodini, *Experimental Techniques*, in print.
- [29] Hutchings, M.T., C. Hipplesey, V. Rainey, *Mat. Res. Sc. Symp Proc.* 166 (1990) 317.
- [30] Reimers, W., p. 159 of ref. [2].
- [31] Reimers, W., p. 263 of ref. [2].

## FIGURE CAPTIONS

- Fig. 1 Schematic representation of the strain measurement by neutron diffraction.
- Fig. 2 Schematic representation of the dedicated neutron diffractometer under construction at LLB, Saclay [14].
- Fig. 3 Definition of the direction of the strain  $\epsilon_{\text{qw}}$  with respect to an arbitrarily chosen reference system within the sample.
- Fig. 4 Strains in a ceramic matrix composite as a function of temperature (Matrix  $\text{Al}_2\text{O}_3$  and whiskers SiC).
- Fig. 5 Lattice strains parallel to the stress applied to a metal matrix composite rod of 20% vol. SiC particulate in an Al (2014) matrix, as obtained by neutron diffraction from different crystallographic planes. The solid lines are obtained by theoretical models [15].
- Fig. 6 a) The elastic strains determined by neutron diffraction for the aluminum matrix (o) and for the silicon carbide reinforcement. b) The total macroscopic strain determined by strain gauges [5].
- Fig. 7 (a) Geometry of a sample of a metal matrix composite (2024 Al alloy matrix reinforced by 25 vol. % SiC particulates); radial distribution of residual stresses in the tangential (b), longitudinal (c) and radial (d) directions [16].
- Fig. 8 Temperature dependence, for both constituents of the sample considered in fig. 9, of the internal stresses in longitudinal (a) and transversal (b) directions [16].
- Fig. 9 Residual stress distribution through a double-V weldment sample of 50 D C-Mn steel. The points refer to neutron measurements and the shaded area to a conventional destructive method [3].
- Fig. 10 (a) Scheme of the experimental device to measure simultaneously 33 points along the incident beam in a T-butt weld specimen [19]; (b) measured distribution of the  $\epsilon_z$  strain component through the plate of fig. 13a: a) at  $z$  0 mm, b) at  $z$  = 8.4 mm, c) at  $z$  = 16.8 mm, d) at  $z$  25.2 mm [11].
- Fig. 11 (a) Weld of AISI 304 stainless steel and geometry of the neutron diffraction experiment (sizes are in mm); (b) map of the iso-strain levels in the  $z$  = 85 mm plane  $\langle 111 \rangle$  direction of the diffracting planes parallel to the X-direction [17].
- Fig. 12 Comparison between tangential strain distribution obtained by neutron diffraction and finite element calculations in a CrMo steel alloy submitted to an internal pressure of 2500 bar [11].
- Fig. 13 The influence of shot peening on fatigue life of a nickel superalloy [18].
- Fig. 14 Schematic representation of the experimental geometry in a neutron diffraction stress scanning through a plate of a shot peened nickel superalloy of 38 x 38 x 12.75 mm dimensions [18].
- Fig. 15 Residual stress field through the plate of fig. 19 [18].
- Fig. 16 Residual stress distribution around a cold expanded hole in a mild steel plate [19].
- Fig. 17 Geometry of residual strain determination in an AISI 316 steel mock-up of the first wall of a thermonuclear fusion reactor submitted to thermal fatigue [20].
- Fig. 18 Theoretical (m, o) and experimental (1, n) values of 34 the residual strains  $c_z$ , (m, 1) and  $F_z$  (o, n) as a function of the depth

along a line from surface to central hole axis; best fit fourth order polynomials for theoretical values [20].

- Fig. 19 Transverse slice and longitudinal plate cut from a railway rail and used for neutron diffraction experiments [21].
- Fig. 20 Longitudinal stresses measured by neutron diffraction down the centre-lines of transverse slice and longitudinal plate samples cut from a used rail (see fig. 24) [21].
- Fig. 21 Residual stress contours in the head of a slice of a used rail. a) transverse stresses; b) vertical stresses [22].
- Fig. 22 a) Geometry of a hot pressed Si<sub>3</sub>N<sub>4</sub> (HPSN) ceramic plate brazed onto an unalloyed steel (St 52) plate, investigated by neutron diffraction. b) Experimental (continuous lines) and calculated (broken lines) residual stress distributions along the central line of the

sample. Arrows indicate results obtained at the surfaces by X-ray diffraction [23].

- Fig. 23 a) Geometry of a plane graphite/molybdenum brazed sample. b) Smoothed stress field versus distance from brazing plane in polycrystalline graphite [25].
- Fig. 24 Comparison between the radial (CYR) and tangential ((YT) residual stress distributions in a plasma semitransferred arc (PTA) coating by neutron and X-ray diffraction [28].
- Fig. 25 Triaxial stress variation with position  $x$  in a cracked fatigue test specimen bolted in the maximum cracktip stress configuration. The arrow denotes the position of the crack-tip on the specimen centre line, and the shaded line the outer edge of the specimen [29].